

# Diffusion of microscopic tracer particles in a yield-stress fluid

Felix K. Opong<sup>a,b</sup>, John R. de Bruyn<sup>a,b,\*</sup>

<sup>a</sup> Department of Physics and Astronomy, University of Western Ontario, London, Ont., Canada N6A 3K7

<sup>b</sup> Department of Physics and Physical Oceanography, Memorial University of Newfoundland, St. John's, Nfld, Canada A1B 3X7

Received 28 February 2006; received in revised form 11 May 2006; accepted 18 May 2006

## Abstract

The motion of micron-sized fluorescent tracer particles in a gel of Carbopol ETD 2050 is studied using fluorescence microscopy. For a Carbopol concentration at which the material shows yield-stress behavior on the bulk scale, the tracer particles display a range of behavior: Some of the particles show slightly subdiffusive behavior, while others are almost completely immobilized. This indicates that the material is inhomogeneous, with different particles sampling different microrheological environments. From our results we calculate the range of microrheological viscous and elastic moduli of the material, which we compare with bulk values of the moduli as determined by conventional shear rheometry.

© 2006 Elsevier B.V. All rights reserved.

*Keywords:* Yield-stress fluids; Microrheology

## 1. Introduction

Yield-stress fluids behave as soft solids when subjected to a shear stress  $\sigma$  less than their yield stress  $\sigma_y$ , but flow when  $\sigma > \sigma_y$ . Such materials have important applications in many areas; examples include pastes and concentrated suspensions, fresh concrete, and foams. Like all soft materials, their complex rheological behavior is a result of structure on scales much larger than the molecular scale [1]. The bulk properties and flow behavior of yield-stress fluids have been studied extensively using shear rheometry [2,3] and a variety of flow experiments [4–10], as well as numerically [11,12]. On the other hand, the microscopic structure of some yield-stress materials has been probed with scattering techniques both at rest and under shear [13–16]. There has been rather little effort, however, aimed at investigating the rheology of yield-stress fluids on the microscopic scale and the interplay between small-scale structure and microrheology in these materials [17]. In this paper we present experimental results on the diffusion of small tracer particles in a Carbopol gel. We demonstrate that the gel is inhomogeneous on the length scale probed by our experiments, and we separate our tracer particles into populations depending on the degree to which their motion is restricted by the gel structure. We then determine the microrheological viscous and elastic moduli for

each population, and contrast our results with bulk rheological measurements.

Various techniques designed to probe the microrheology – that is, the viscoelastic response of complex fluids on the microscopic scale – have been developed over the last decade [18–22]. Microrheological methods typically involve measurements of the motion of small (sub-micron diameter) particles suspended in the material of interest. Passive microrheology is based on the determination of viscoelastic parameters from measurements of the mean squared displacement  $\langle r^2(\tau) \rangle$  of the particles as a function of a lag time  $\tau$ .  $\langle r^2(\tau) \rangle$  can be measured with light scattering techniques [23–26] or by directly tracking the trajectories of the tracer particles using video microscopic techniques [27–31]. Active microrheology, on the other hand, involves measurement of the response of a small particle to an external force [35–39].

Microrheological methods in general require a much smaller sample than needed for conventional shear rheometry, so they are useful for characterizing materials which are expensive or which cannot be obtained in large quantities, such as some biological fluids. In these applications, one typically wants the microscopic measurements to give the bulk viscoelastic properties, which requires that the fluid under study be homogeneous on the length scales probed by the experiments. This has been shown to be the case for several complex fluids, including solutions of poly(ethylene oxide), an uncross-linked linear chain polymer [23,24,30]; a suspension of hard-sphere silica particles in ethylene glycol [24]; an oil-in-water emulsion [24,25]; and cross-linked polyacrylamide sols and gels [34].

\* Corresponding author.

E-mail address: [debruy@uwo.ca](mailto:debruy@uwo.ca) (J.R. de Bruyn).

In contrast, if the size of the suspended particles is smaller than the size of local inhomogeneities in the material properties, then individual particles will experience different local microrheological environments. In such cases, microrheology provides a tool that can be used to investigate structure and rheology on these small scales. The microrheology of networks of F-actin, a protein which is a major structural component of cell membranes, has been studied in some detail [26,27,29–31,33] using light scattering as well as particle-tracking and two-particle correlation measurements. It has been found that microrheological measurements agree well with bulk measurements if the suspended particles are larger than the mesh size of the actin network. When the particle size is comparable to the mesh size, however, the rheology becomes dependent on the length scale sampled by the tracer particles as they diffuse [27,32,33].

Passive microrheological measurements give the mean squared displacement of small particles moving in a viscoelastic material due to thermal fluctuations. The microscopic viscous and elastic moduli are extracted from the mean squared displacement under the assumption that the Stokes–Einstein relation that is valid for purely viscous Newtonian fluids can be generalized to viscoelastic fluids with frequency-dependent linear viscoelastic moduli [22,24]. It is also assumed that inertial effects on the motion of the probe particles are negligible. The method by which the viscoelastic moduli are calculated has been described by Mason [22]. Briefly, we define  $\alpha(\omega)$  to be the frequency-dependent logarithmic slope of the mean squared displacement, evaluated at a frequency  $\omega$  equal to the reciprocal of the lag time:

$$\alpha(\omega) = \left. \frac{d \ln \langle r^2(\tau) \rangle}{d \ln \tau} \right|_{\tau=1/\omega} \quad (1)$$

The magnitude of the mechanical modulus  $G(\omega)$  is then

$$|G(\omega)| = \frac{k_B T}{\pi a \langle r^2(1/\omega) \rangle \Gamma(1 + \alpha(\omega))}. \quad (2)$$

Here  $k_B$  is the Boltzmann constant,  $T$  the temperature,  $a$  the radius of the suspended particles, and  $\Gamma$  the Gamma function. The viscous and elastic moduli,  $G''$  and  $G'$ , respectively, are given by

$$G''(\omega) = |G(\omega)| \sin \left( \frac{\pi \alpha(\omega)}{2} \right) \quad (3)$$

and

$$G'(\omega) = |G(\omega)| \cos \left( \frac{\pi \alpha(\omega)}{2} \right). \quad (4)$$

Here we study the microrheology of a Carbopol gel. When dispersed in water, Carbopol forms a transparent gel whose rheological properties can be tuned by varying the Carbopol concentration and pH. Steric interactions among swollen microgel particles and cross-links between polymer chains in the material give rise to a yield stress [40–45]. The high degree of transparency of Carbopol gels, the relative unimportance of aging [46,47] in these materials, along with the ease with which samples can be prepared, has led to the use of Carbopol gels as model yield-stress fluids [4,8,45].

In a previous paper [17], we presented the results of both particle tracking and dynamic light scattering measurements of the microrheology of Carbopol gels as a function of Carbopol concentration. We showed that the microrheological moduli were several orders of magnitude smaller than the moduli determined from bulk shear rheometry. We also demonstrated that the gels were inhomogeneous on the length scale probed by our measurements, so that individual tracer particles sampled different microscopic rheological environments.

In the present paper we look in more detail at the variations in microrheological environment for a sample with a Carbopol concentration of 0.5 wt.%. This material is a stiff gel on the bulk scale, but we find that while some of the suspended tracer particles are more-or-less completely immobilized by the gel, others diffuse almost freely. We separate our tracer particles into populations depending on their mean squared displacements and study the behavior of each population.

The remainder of this paper is organized as follows. In Section 2 we present the experimental details. Our results are presented in Section 3 and discussed in Section 4. Section 5 is a brief conclusion.

## 2. Experiment

Our experiments were performed using Carbopol ETD 2050, which consists of polymers based on polyacrylic acid, crosslinked with a polyalkenyl polyether [44]. Samples were prepared in a dust free environment. Fluorescent latex microspheres 0.49  $\mu\text{m}$  in diameter, with density 1.05  $\text{g}/\text{cm}^3$  and refractive index 1.59 at 589 nm were obtained as a suspension in water [48]. These microspheres contained a dye which fluoresced in the red when excited with green light. They were sonicated in an ultrasonic bath to disperse any clumps prior to use, then diluted with deionized water to give a sphere volume fraction of typically  $5 \times 10^{-5}$ . Carbopol powder was added slowly to the continuously stirred dilute sphere suspension to a concentration of 1.2 wt.%. The resulting dispersion had a pH of about 3. Sodium hydroxide solution was added to raise the pH to 6. Gel samples of the desired Carbopol concentration  $c$  were obtained by diluting this stock solution with additional water/sphere suspension (and readjusting the pH to 6 if necessary); most of the results reported here were obtained with  $c = 0.5$  wt.%. Any air bubbles were removed by centrifugation. Samples used for rheological measurements were prepared the same way but without the microspheres.

Our particle-tracking apparatus has been described elsewhere [17]. Samples containing the fluorescent microspheres were loaded into a sample cell 10 mm  $\times$  10 mm  $\times$  0.75 mm high which was sealed with a silicone-based grease. The cell was mounted on the stage of an Olympus BX50Wi upright epillumination fluorescence microscope with an overall magnification of 150 $\times$  which was focused on the mid-point of the cell, giving a resolution of 0.27  $\mu\text{m}/\text{pixel}$ . The samples were allowed to equilibrate for half an hour at room temperature before measurements were made. Typically from 50 to 100 fluorescent spheres were visible in the field of view at any time. Images of the spheres were captured with a 640 pixel  $\times$  480 pixel CCD

camera, corresponding to a field of view of  $175 \mu\text{m} \times 131 \mu\text{m}$ , which is much larger than both the suspended fluorescent particles and the expected scale of the structure in the material. Images were recorded at the standard video frame rate of 30 frames per second with a VCR for runs which were typically 10–20 min in length. After they were recorded, a frame grabber in a personal computer was used to digitize the images at frame rates ranging from 2 to 15 frames per second. The frame rate was chosen as a compromise between the need to obtain data for a large range of lag times and the amount of memory in our computer.

We used the particle tracking software described in [49,50] to process images, to determine the particle locations in each video frame, and to analyze the particle trajectories from frame to frame. The images were calibrated with an etched calibration slide, and the uncertainty in the particle positions was found to be  $\pm 0.02 \mu\text{m}$  by imaging immobile particles [51]. Fluctuations in temperature, which were on the order of  $0.1^\circ\text{C}$  over the course of a run, contribute an additional relative uncertainty of  $\pm 0.03\%$  to  $\langle x^2 \rangle$ , which is negligible compared to the uncertainty due from the imaging system. Our imaging system records video frames in the form of two interleaved fields recorded at a rate of 60 fields per second. Since the motion of the particles in the time between fields can be significant, we used individual fields rather than entire frames when digitizing the images. As a result, our spatial resolution was higher in the direction parallel to the video scan lines (referred to as the  $x$ -direction) than in the perpendicular ( $y$ ) direction, so we calculated the one-dimensional mean squared displacement  $\langle x^2 \rangle$  in the  $x$ -direction only.

Oscillatory and steady shear measurements of the bulk rheological properties of our Carbopol samples were made at  $25^\circ\text{C}$  with an Ares RHS controlled strain rheometer. We used parallel plate tools 5 cm in diameter with a gap of 1 mm. Fine sandpaper was glued to the surfaces of both plates to eliminate wall slip.

### 3. Results

Fig. 1 shows the results of bulk rheological measurements on Carbopol gels. Fig. 1(a) shows a flow curve for  $c = 0.5\%$ . It displays the expected yield stress behavior, approaching a constant value at low shear rates. The dashed line through the points is a fit to a Herschel–Bulkley model,

$$\sigma = \sigma_y + K\dot{\gamma}^n, \quad (5)$$

where  $\sigma$  is the shear stress,  $\dot{\gamma}$  the strain rate, and  $K$ ,  $n$ , and the yield stress  $\sigma_y$  are treated as fitting parameters. The fit describes the data reasonably well. The results of oscillatory shear measurements are presented in Fig. 1(b) as a function of angular frequency, again for  $c = 0.5\%$ . The amplitude of the applied strain was 1%, which was within the linear regime for this material. The elastic modulus is much larger than the viscous modulus over the range of frequencies accessible to our rheometer, indicating that the Carbopol behaves as a soft elastic solid for small strains, again consistent with yield-stress behavior. The yield stress, determined from fits like that shown in Fig. 1(a), is plotted as a function of Carbopol concentration  $c$  in Fig. 11 below. These rheometric measurements confirm that

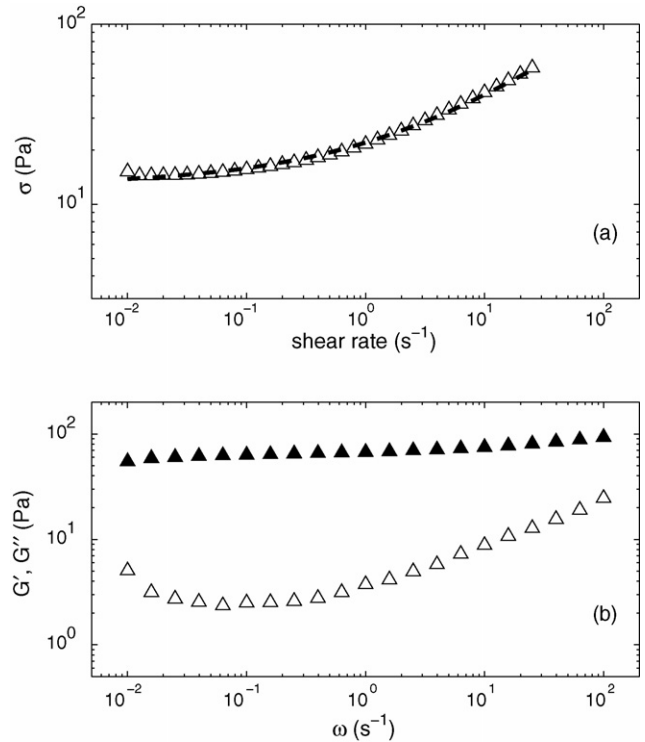


Fig. 1. The bulk-scale rheology of 0.5 wt.% Carbopol gels measured with a shear rheometer. (a) The flow curve measured under steady shear. The dashed line is a fit to the Herschel–Bulkley model, Eq. (5). (b) The elastic (solid symbols) and viscous (open symbols) moduli as a function of frequency, measured under oscillatory strain with an amplitude of 1%.

the Carbopol gels we study are yield stress fluids on the bulk scale.

Our results on the microrheology of Carbopol for a range of concentrations have been presented elsewhere [17]; here we focus on a detailed analysis of the motion of the small tracer particles at  $c = 0.5 \text{ wt.}\%$ . At this concentration the material is a very stiff gel with a yield stress of 12.8 Pa. Three individual particle trajectories measured in a single sample at this concentration are shown in Fig. 2, which illustrates the range of behavior observed. Some particles, like that corresponding to the trajectory labeled (c) in Fig. 2, are almost immobile. Others, like that with trajectory (a), move relatively freely. Even in the latter case, however, the motion of the particle is clearly very different from the random walk expected for simple Brownian diffusion. Rather, the particle spends a substantial period more or less confined to one region, then wanders over to another region where again it becomes confined for a time.

Fig. 3 shows the one-dimensional squared displacement  $x^2(\tau)$  as a function of the lag time  $\tau$  for each of the particles tracked during a run with a single sample of concentration  $c = 0.5\%$ .  $\tau$  for each particle is measured from the time at which it first entered the experimental field of view. The straight dotted line corresponds to  $x^2 \propto \tau$ , which is the expected behavior for normal diffusion. The observed particle motions are in general subdiffusive, with  $x^2(\tau)$  having a logarithmic slope  $\alpha$  which is less than 1. For some particles, the motion is nearly completely diffusive, while others are almost completely trapped. These results show that the sample is strongly inhomogeneous on the scale

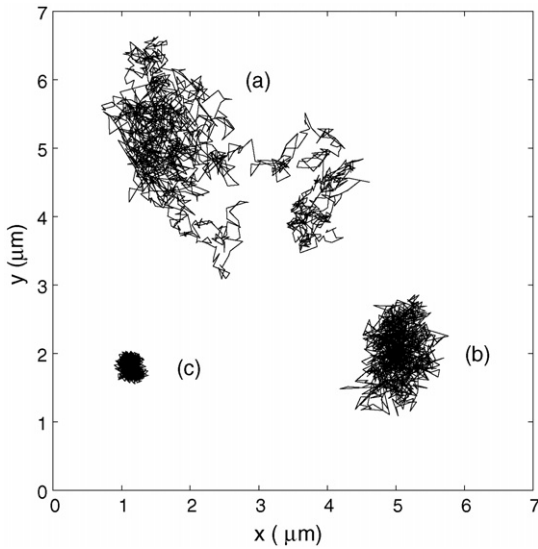


Fig. 2. Three individual particle trajectories for  $c = 0.5\%$ .

probed by the particles: different particles experience different local rheological environments.

To study this further, we divided the particles into three populations based (arbitrarily) on their value of  $x^2$  at  $\tau = 10$  s. These three sets of particles are indicated by the different line styles in Fig. 3. The particles in population I, shown as dashed lines, move relatively freely. For these particles,  $\alpha$  is slightly smaller than one for  $\tau \lesssim 10$  s, then decreases for higher  $\tau$ . Population III particles, shown as solid lines, move very little— $x^2$  is essentially flat out to  $\tau = 10$  s, but in some cases shows a slight increase at larger lag times. Population II is intermediate between the other two populations, with the squared displacement increasing subdiffusively at short lag times then becoming almost constant for  $\tau > 10$  s. The distribution of values of  $x^2$  ( $\tau = 10$  s) for all of the particles plotted in Fig. 3 is shown in the inset to Fig. 3, with the vertical dashed lines indicating the boundaries between populations. By averaging  $x^2$  over all particles in each of the three populations, we obtain the mean squared displacements for

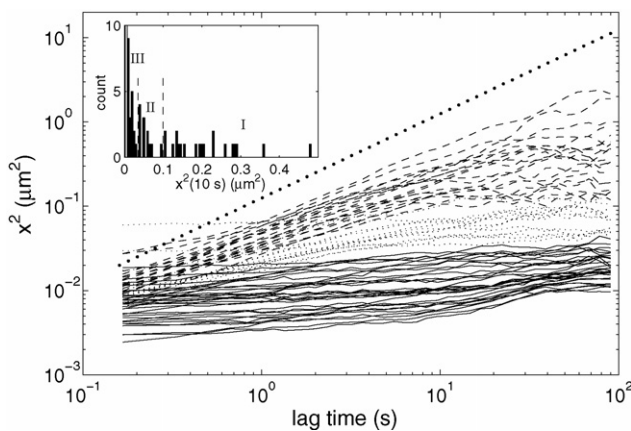


Fig. 3.  $x^2(\tau)$  for all particles tracked in a gel with concentration  $c = 0.5\%$ . The different line styles indicate how the particles were divided into populations based on the value of their squared displacement at  $\tau = 10$  s. The inset is a histogram showing the distribution of  $x^2(\tau = 10$  s), with the vertical dashed lines marking the boundaries between the three populations.

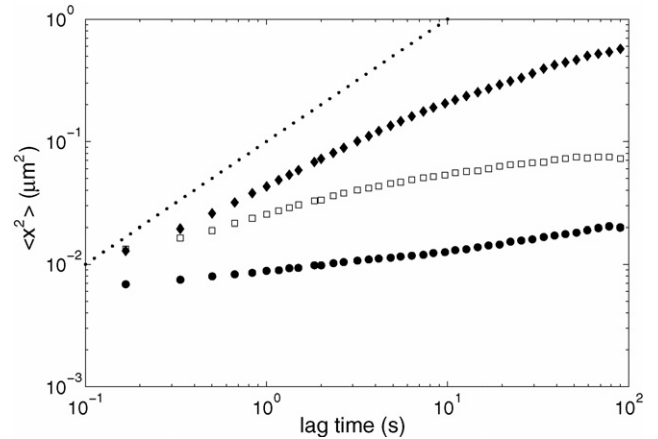


Fig. 4. The mean squared displacement calculated for each of the three populations at  $c = 0.5\%$ . The dotted line has a logarithmic slope of 1 as expected for unrestricted diffusion and is shown for comparison. Diamonds: population I; squares, population II; circles, population III.

each population. These quantities are shown as a function of  $\tau$  in Fig. 4.

Fig. 5 shows the distribution of the particle displacements (termed the van Hove correlation function) in a time interval of 1 s for each population. The inset shows the distribution for all of the particles taken together. For unrestricted diffusion in a homogeneous medium one would expect a Gaussian distribution. The curves in Fig. 5 are fits of the data for the three populations to Gaussians. The fits describe the distributions reasonably well, although there are small but systematic deviations at larger displacements. The width of the distribution decreases as we go from populations I to III, giving the reasonable result that the effective diffusion coefficient of the material is smaller for particles whose motion is more strongly restricted. When all of the particles are considered together, however, the distribution is not well described by a Gaussian, and indeed appears closer to an exponential distribution in this particular case.

The deviations of the distribution of displacements from a Gaussian can be quantified by a parameter  $N$  which compares

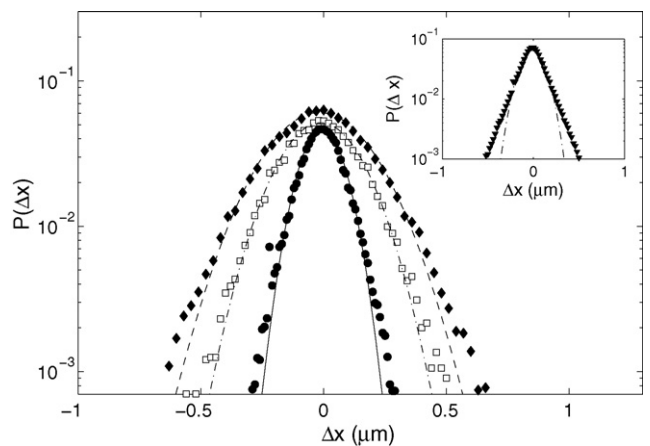


Fig. 5. The distribution of particle displacements for a lag time  $\tau$  of 1 s for the three populations of particles at  $c = 0.5\%$ . As in Fig. 4, diamonds represent population I; squares, population II; and circles, population III. The lines through the data are fits to Gaussian distributions. The inset shows the distribution for all particles together (downward triangles), along with a Gaussian fit.

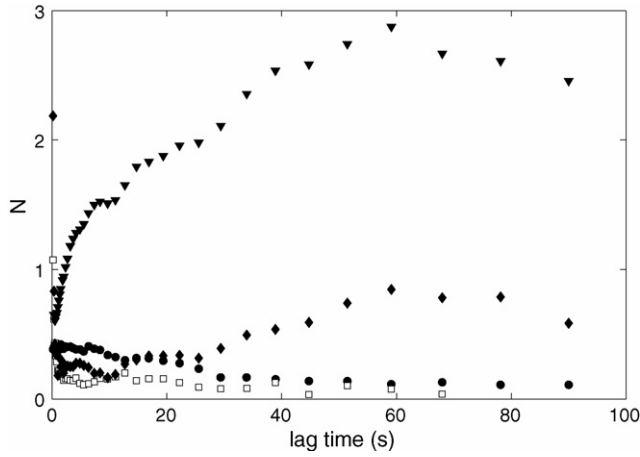


Fig. 6. The non-Gaussian parameter defined in the text for the three populations at  $c = 0.5\%$ , with diamonds representing population I; squares, population II; and circles, population III. The non-Gaussian parameter for all particles taken together is indicated by the downward triangles.

the fourth moment of the distribution to the second moment [52]:

$$N = \frac{\langle x^4 \rangle}{3\langle x^2 \rangle^2} - 1. \quad (6)$$

This quantity is zero for a Gaussian distribution, while a positive value indicates a sharper and more strongly peaked distribution.  $N$  is plotted for each of the three populations as well as for all particles together in Fig. 6. When all particles are taken together, the non-Gaussian parameter is large, reaching a maximum near  $\tau = 60$  s. For the three populations, however,  $N$  is substantially smaller, since the van Hove correlation functions are much closer to Gaussian distributions, and for populations II and III the non-Gaussian parameter seems to approach zero as  $\tau$  becomes long.

Fig. 7 shows the trapping of the particles in a different way [53,54]. If a particle is executing a random walk, then its motion in the interval from time  $t_0$  to  $t_1 = t_0 + \tau$  will be uncorrelated with its motion from  $t_1$  to  $t_2 = t_1 + \tau$ . On the other hand, if the particle is trapped in a cage and approaches the wall of that cage in the first time interval, then it may bounce off and move away from the wall in the next interval. In this case the direction of motion in the second interval will, on average, have a component in the opposite direction to the motion in the first interval. In Fig. 7 we plot on the abscissa the distance  $r_{01}$  moved in the first time interval, while the ordinate is  $\langle x_{12} \rangle$ , the mean of the component of the motion in the second time interval parallel to  $\vec{r}_{01}$ . Here the length of the interval is  $\tau = 1$  s. Data for the three populations with  $c = 0.5\%$  are plotted. All show a strong negative correlation, indicative of caging effects. At low  $r_{01}$  the data can be described by  $\langle x_{12} \rangle = -br_{01}$ , where  $b$ , the magnitude of the slope, can be interpreted as a measure of the strength of the cage. Not surprisingly, our data show that the caging effect becomes more pronounced, that is,  $b$  becomes larger, as the motion of the particles becomes more restricted.

Fig. 8 shows how the ‘‘cage strength’’  $b$  varies with  $\langle x^2 \rangle^{1/2}$ , the root mean square distance probed by the particles. Here  $\langle x^2 \rangle^{1/2}$  is determined for each population for several different values of the lag time  $\tau$ . We see that  $b$  increases roughly linearly with  $\langle x^2 \rangle^{1/2}$ , indicating that the effect of the gel on the parti-

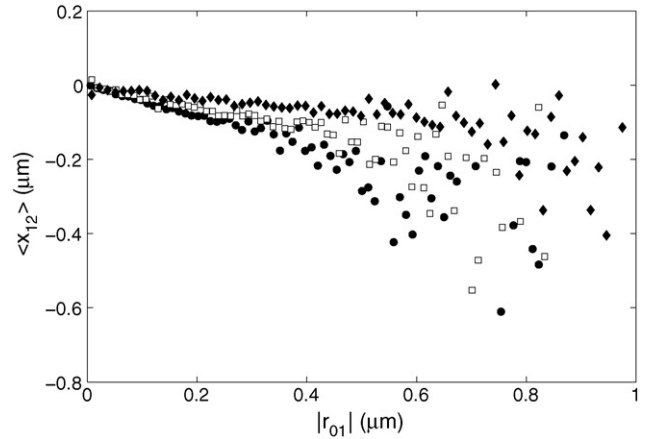


Fig. 7. Correlation analysis for the three populations at  $c = 0.5\%$  and  $\tau = 1$  s. The symbols indicate the different populations as in previous figures: diamonds: population I; squares, population II; circles, population III.

cles’ motion becomes stronger as the particles explore larger distances.

The microrheological elastic and viscous moduli, determined from the mean squared displacements for the three populations of particles using Eqs. (4) and (3), are plotted as a function of frequency in Fig. 9. In calculating  $G'$  and  $G''$  in this way, we have assumed that  $\langle r^2 \rangle = 3\langle x^2 \rangle$ , i.e., that the motion of the particles is isotropic. We fit a smooth function to the data plotted in Fig. 4 and used that fitting function to calculate the moduli. For population I, those particles that move most freely, the viscous modulus is about a factor of two larger than the elastic modulus at high frequencies. The data for this population show a crossover at  $\omega \approx 0.04$  s $^{-1}$ , below which the elastic modulus becomes dominant. This is in direct contrast to the bulk rheological results, and indicates that over short times, these particles see a material that is predominantly viscous on the microscopic scale. On the other hand, population III, the most strongly restricted particles, see an elastic modulus that is about three times larger than the viscous modulus over the entire frequency range probed in our experiments. Population II similarly sees an elas-

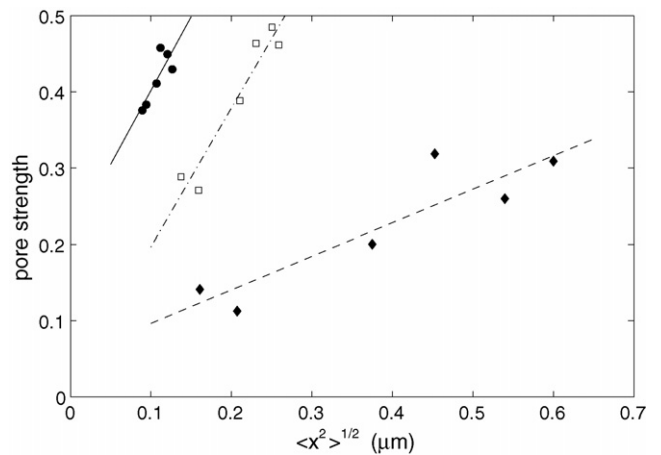


Fig. 8. Pore strength as determined from the slope of the data in Fig. 7, plotted as a function of the rms displacement of the particles. The symbols have the same meanings as in previous figures. The lines are straight lines fit to the data for each population.

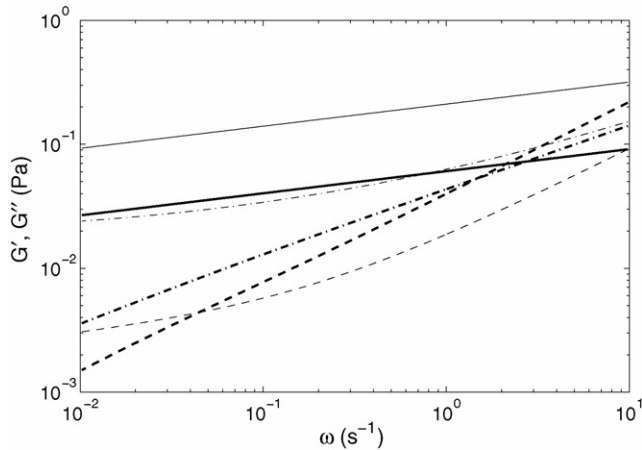


Fig. 9. The frequency-dependent moduli determined from the mean squared displacement for each of the three populations of particles. The lighter lines correspond to the elastic modulus  $G'$  and the heavy lines to the viscous modulus  $G''$ . The different line types indicate the different populations: dashed, population I, dot-dashed, population II, and solid, population III.

tic material at all frequencies, with the suggestion of a crossover at  $\omega \gtrsim 10 \text{ s}^{-1}$ , just outside the range of our experimental data.

The dynamic viscosity  $\eta = G''/\omega$  seen by the different populations is plotted in Fig. 10, along with the viscosity determined from the bulk rheology measurements. The bulk viscosity diverges as  $\omega$  goes to zero approximately as  $1/\omega$ , as expected for a material with a bulk yield stress. The viscosities on the micron scale are approximately two orders of magnitude smaller than the bulk viscosities, but still substantially larger than the viscosity of water. The microscopic viscosities also appear to diverge as the frequency goes to zero. In the case of population III  $\eta$  is again approximately proportional to  $1/\omega$ , but the less confined populations show a weaker divergence.

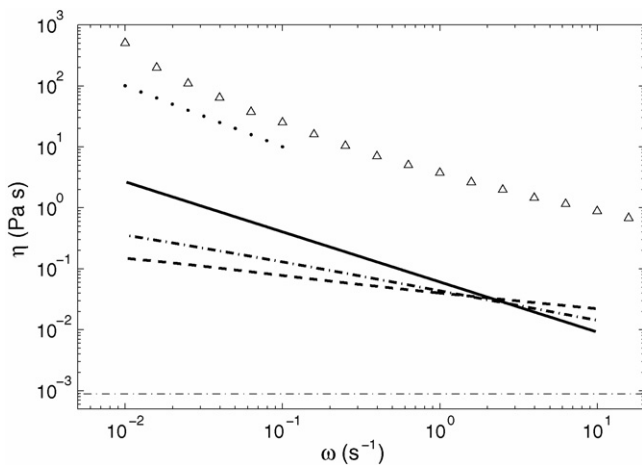


Fig. 10. The heavy lines show the viscosities seen by the three populations of particles, determined from the microrheological viscous moduli plotted in Fig. 9. The different line types indicate the different populations as in Fig. 9. The symbols are the viscosity of the bulk material determined from the shear rheometry data shown in Fig. 1. The viscosity of water is shown as the light dot-dashed line, and the dotted line shows a  $1/\omega$  frequency dependence for comparison.

#### 4. Discussion

On the bulk scale a Carbopol gel at a concentration of 0.5 wt.% has a yield stress of several Pa. The results presented here, however, show clearly that the carbopol gels are inhomogeneous on the micron scale. Different suspended tracer particles see different microrheological environments, as evidenced by the wide variation in behavior observed within a single sample. Some of the particles are quite mobile, with a squared displacement that is only slightly subdiffusive. The microscopic environment experienced by this population of particles is close to that of a viscous fluid. In contrast, other particles are essentially immobile and see an environment that is predominantly elastic.

The distributions of step sizes for the three populations we have identified in the sample studied here are much more closely described by Gaussian distributions than is the case when all of the particles are taken together [17]. The deviations from the Gaussian fits observed at higher values of  $\Delta x$  in Fig. 5 are real, however, and are a sign that the motion of the tracer particles is not purely diffusive and that the material is heterogeneous. Similarly, the non-Gaussian parameter is much smaller for the individual populations than for all of the particles together.

In our earlier work [17], when we studied all of the particles tracked in gels of different concentrations, as well as in previous work on caging in complex fluids [54], the negative linear correlation observed in Fig. 7 breaks down above a particular value of  $r_{01} = \ell$ . This value, added to the particle diameter, was taken as the characteristic cage size  $d$ . In [17] we found  $\ell \approx 0.27 \text{ }\mu\text{m}$  and  $d \approx 0.76 \text{ }\mu\text{m}$  for  $c = 0.5\%$ . In the present case, however, there is no obvious break point in the linear relationship between  $\langle x_{12} \rangle$  and  $r_{01}$ . The data plotted in Fig. 7 become noisier above about  $r_{01} \approx 0.5 \text{ }\mu\text{m}$ , but this is simply due to the fact that there are fewer particles to average over when  $r_{01}$  is this large.

It is possible, but unlikely, that the characteristic length scale of the cages is larger than the distances probed by our particles, but our data show no break in the slope of the plot of  $\langle x_{12} \rangle$  versus  $r_{01}$  for  $\tau$  up to 30 s. Alternatively, it may be that the cages, in fact, have no characteristic length scale—the distribution of pores within the gel may have a fractal structure on the scales probed by our experiments. We have observed similar behavior in experiments on laponite clay suspensions [55], in which case light scattering measurements also suggest that the material has a fractal structure over a range of length scales [13–15].

The effective cage strength determined from the correlation analysis, plotted in Fig. 8, increases with the distance probed by the particles. In this sense the effect of the cages is to act as a restoring force on the particles, keeping them confined to a particular region of the material.

The range of behavior of the tracer particles is due to inhomogeneities in the material structure on the length scales probed by our experiments. The microrheological parameters plotted in Fig. 10 confirm that the populations II and III particles see a material that is locally elastic while population I particles experience local rheological environments that are primarily viscous. Even in the case of population I we observe a crossover at low frequencies, below which the elastic modulus dominates. This suggests that elasticity dominates on long time scales, even for

the most mobile particles. This is also indicated by the plateaus in the squared displacements of the individual particles seen at long times in Fig. 3.

We note that the crossover in moduli seen in our microrheological data is opposite to that typically seen in the traditional shear rheology of polymers [1] or in microrheological measurements on F-actin [26]. In these instances, the material is viscous over long time scales but elastic on short times due to entanglement of the polymer molecules. In our case, the gel is viscous at short times but elastic at long times due to the restriction of the particle motion caused by the gel structure.

An important issue is whether the gel displays a true yield stress on the microscopic scale. The dominance of the elastic modulus and the nearly  $-1/\omega$  divergence of the microscopic viscosity in the case of population III, the most strongly confined particles, suggests these particles do see a microscopic yield stress. The situation is less clear for the more freely-moving particles in population I. In this case the microscopic viscosity diverges more slowly and the microrheological environment becomes elastic only at the lowest frequencies studied. Further experiments are needed to address this question fully. More information on the length-scale dependence of the structure and viscoelastic properties could be obtained from two-particle microrheology, that is, by studying the correlations between pairs of tracer particles as a function of the pair separation [56,57].

Finally, one would like to understand the relationship between the small-scale properties studied in our particle tracking experiments and the bulk rheological properties of the material. While we are not yet close to that goal, we show in Fig. 11 a

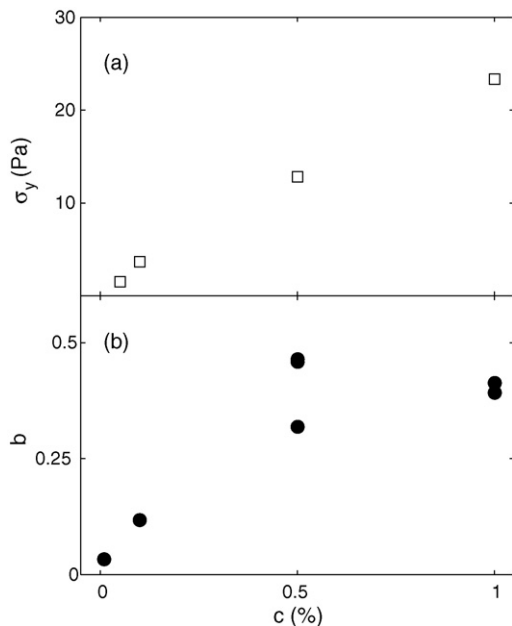


Fig. 11. (a) The yield stress of Carbopol dispersions plotted as a function of Carbopol concentration  $c$ . These data were determined from flow curves measured with a shear rheometer, as in Fig. 1. (b) The cage strength  $b$  determined from a correlation analysis of the particle trajectories, as in Fig. 7, plotted as a function of  $c$  for a lag time  $\tau = 1$  s. When more than one data point is shown at a given concentration, the particles were split into populations based on their degree of mobility, as discussed in detail for  $c = 0.5\%$  in the text.

comparison between the cage strength  $b$  determined from microrheological measurements, and the yield stress  $\sigma_y$  determined from bulk rheology. The concentration dependence of the two quantities is similar, perhaps suggesting a starting point for a more complete understanding of the connection between bulk and microrheological properties.

## 5. Conclusion

We have used multiple particle tracking microrheology to study the small-scale viscoelastic properties of a Carbopol gel with a bulk yield stress. While some of the suspended tracer particles undergo slightly subdiffusive motion, others are almost completely immobilized. This indicates that the material is inhomogeneous, with different particles sampling different microrheological environments. From the microscopic viscous and elastic moduli, we find that the most mobile particles experience a predominantly viscous environment at high frequencies, with a crossover to an elastic behavior at the lowest frequencies studied. In contrast, the most strongly trapped particles experience an elastic environment at all frequencies. Our results suggest that these trapped particles, at least, see a yield stress on the microscopic scale.

## Acknowledgments

This research was supported by the Canadian Space Agency and the Natural Science and Engineering Research Council of Canada. We acknowledge the collaboration of B. Frisken, A. Bailey, and L. Rubatat on aspects of this research. We thank M. Goldsworthy for technical assistance.

## References

- [1] R.G. Larson, *The Structure and Rheology of Complex Fluids*, Oxford University Press, New York, 1999.
- [2] A. Magnin, J.M. Piau, Cone and plate rheometry of fluids with a yield stress. Study of an aqueous gel, *J. Non-Newtonian Fluid Mech.* 36 (1990) 85.
- [3] N.J. Alderman, G.H. Meeten, J.D. Sherwood, Vane rheometry of bentonite gels, *J. Non-Newtonian Fluid Mech.* 39 (1991) 291.
- [4] D.D. Atapattu, R.P. Chhabra, P.H.T. Uhlherr, Wall effect for spheres falling at small Reynolds number in a viscoplastic medium, *J. Non-Newtonian Fluid Mech.* 38 (1990) 31; D.D. Atapattu, R.P. Chhabra, P.H.T. Uhlherr, Creeping sphere motion in Herschel–Bulkley fluids: flow field and drag, *J. Non-Newtonian Fluid Mech.* 59 (1995) 245.
- [5] B.J. Briscoe, P.F. Luckham, S.R. Ren, An assessment of a rolling-ball viscometer for studying non-Newtonian fluids, *Coll. Surf.* 62 (1992) 153.
- [6] P. Coussot, *Mudflow Rheology and Dynamics*, Balkema, Rotterdam, 1997.
- [7] B.S. Gardiner, B.Z. Dlugogorski, G.J. Jameson, R.P. Chhabra, Yield stress measurements of aqueous foams in the dry limit, *J. Rheol.* 42 (1998) 1437.
- [8] L. Jossic, A. Magnin, Drag and stability of objects in a yield stress fluid, *AIChE J.* 47 (2001) 2666.
- [9] J.R. de Bruyn, P. Habdas, S. Kim, Fingering instability of a sheet of yield-stress fluid, *Phys. Rev. E* 66 (2002) 031504.
- [10] N.P. Chafe, J.R. de Bruyn, Drag and relaxation in a Bentonite clay suspension, *J. Non-Newtonian Fluid Mech.* 130 (2005) 129.
- [11] A.N. Beris, J.A. Tsamopoulos, R.C. Armstrong, R.A. Brown, Creeping motion of a sphere through a Bingham plastic, *J. Fluid Mech.* 158 (1985) 219.

- [12] J. Blackery, E. Mitsoulis, Creeping motion of a sphere in tubes filled with a Bingham plastic material, *J. Non-Newtonian Fluid Mech.* 70 (1997) 59.
- [13] F. Pignon, J.-M. Piau, A. Magnin, Structure and pertinent length scale of a discotic clay gel, *Phys. Rev. Lett.* 76 (1996) 4857.
- [14] F. Pignon, A. Magnin, J.-M. Piau, Butterfly light scattering pattern and rheology of a sheared thixotropic clay gel, *Phys. Rev. Lett.* 79 (1997) 4689.
- [15] F. Pignon, A. Magnin, J.-M. Piau, Thixotropic behavior of clay dispersions: combinations of scattering and rheometric techniques, *J. Rheol.* 42 (1998) 1349.
- [16] D. Bonn, H. Kellay, H. Tanaka, G.H. Wegdam, J. Meunier, Laponite: what is the difference between a gel and a glass? *Langmuir* 15 (1999) 7534.
- [17] F.K. Oppong, L. Rubatat, A.E. Bailey, B.J. Frisken, J.R. de Bruyn, Microrheology and structure of a polymer gel, *Phys. Rev. E* 73 (2006) 041405.
- [18] F.C. MacKintosh, C.F. Schmidt, *Microrheology*, *Curr. Opin. Coll. Interf. Sci.* 4 (1999) 300.
- [19] M.J. Solomon, Q. Lu, Rheology and dynamics of particles in viscoelastic media, *Curr. Opin. Colloid Interf. Sci.* 6 (2001) 430.
- [20] T.A. Wagh, *Microrheology of complex fluids*, *Rep. Prog. Phys.* 68 (2005) 685.
- [21] M.L. Gardel, M.T. Valentine, D.A. Weitz, *Microrheology*, in: K. Breuer (Ed.), *Microscale Diagnostic Techniques*, Springer, New York, 2005.
- [22] T.G. Mason, Estimating the viscoelastic moduli of complex fluids using the generalized Stokes–Einstein equation, *Rheol. Acta* 39 (2000) 371.
- [23] B.R. Dasgupta, S.-Y. Tee, J.C. Crocker, B.J. Frisken, D.A. Weitz, Microrheology of polyethylene oxide using diffusing wave spectroscopy and single scattering, *Phys. Rev. E* 65 (2002) 051505.
- [24] T.G. Mason, D.A. Weitz, Optical measurements of frequency-dependent linear viscoelastic moduli of complex fluids, *Phys. Rev. Lett.* 74 (1995) 1250.
- [25] T.G. Mason, H. Gang, D.A. Weitz, Rheology of complex fluids measured by dynamic light scattering, *J. Mol. Struct.* 383 (1996) 81.
- [26] T. Gisler, D.A. Weitz, Scaling the microrheology of semidilute F-actin solutions, *Phys. Rev. Lett.* 82 (1999) 1606.
- [27] I.Y. Wong, M.L. Gardel, D.R. Reichman, E.R. Weeks, M.T. Valentine, A.R. Bausch, D.A. Weitz, Anomalous diffusion probes microstructure dynamics of entangled F-actin networks, *Phys. Rev. Lett.* 92 (2004) 178101.
- [28] T.G. Mason, K. Ganesan, J.H. van Zanten, D. Wirtz, S.C. Kuo, Particle tracking microrheology of complex fluids, *Phys. Rev. Lett.* 79 (1997) 3282.
- [29] Y. Tseng, D. Wirtz, Mechanics and multiple particle tracking microheterogeneity of  $\alpha$ -actinin crosslinked actin filament networks, *Biophys. J.* 81 (2001) 1643.
- [30] M.T. Valentine, P.D. Kaplan, D. Thota, J.C. Crocker, T. Gisler, R.K. Prud'homme, M. Beck, D.A. Weitz, Investigating the microenvironments of inhomogeneous soft materials with multiple particle tracking, *Phys. Rev. E* 64 (2001) 061506.
- [31] M.L. Gardel, M.T. Valentine, J.C. Crocker, A.R. Bausch, D.A. Weitz, Microrheology of entangled F-actin solutions, *Phys. Rev. Lett.* 91 (2003) 158302.
- [32] D.T. Chen, E.R. Weeks, J.C. Crocker, M.F. Islam, R. Verma, J. Gruber, A.J. Levine, T.C. Lubensky, A.G. Yodh, Rheological microscopy: local mechanical properties from microrheology, *Phys. Rev. Lett.* 90 (2003) 108301.
- [33] J. Liu, M.L. Gardel, K. Kroy, E. Frey, B.D. Hoffman, J.C. Crocker, A.R. Bausch, D.A. Weitz, Microrheology probes length scale dependent rheology, *Phys. Rev. Lett.* 96 (2006) 118104.
- [34] B.R. Dasgupta, D.A. Weitz, Microrheology of cross-linked polyacrylamide networks, *Phys. Rev. E* 71 (2005) 021504.
- [35] F. Ziemann, J. Radler, E. Sackmann, Local measurements of viscoelastic moduli of entangled actin networks using an oscillating magnetic bead micro-rheometer, *Biophys. J.* 66 (1994) 2210.
- [36] F.G. Schmidt, F. Ziemann, E. Sackmann, Shear field mapping in actin networks by using magnetic tweezers, *Eur. Biophys. J.* 24 (1996) 348.
- [37] F. Amblard, A.C. Maggs, B. Yurke, A.N. Pargellis, S. Leibler, Subdiffusion and anomalous local viscoelasticity in actin networks, *Phys. Rev. Lett.* 77 (1996) 4470.
- [38] H.D. Ou-Yang, Design and applications of oscillating optical tweezers for direct measurements of colloidal forces, in: R.S. Farinato, P.L. Dubin (Eds.), *Colloid–Polymer Interactions: From Fundamentals to Practice*, Wiley, New York, 1999.
- [39] K.C. Neuman, S.M. Block, Optical trapping, *Rev. Sci. Instr.* 75 (2004) 2787.
- [40] Noveon technical data sheet #216, <http://www.pharma.noveon.com/literature/tds/tds216.pdf>, 2002.
- [41] R.J. Ketz Jr., R.K. Prud'homme, W.W. Graessley, Rheology of concentrated microgel solutions, *Rheol. Acta* 27 (1988) 531.
- [42] J.O. Carnali, M.S. Naser, The use of dilute solution viscometry to characterize the network properties of carbopol microgels, *Colloid Polym. Sci.* 270 (1992) 183.
- [43] G.P. Roberts, H.A. Barnes, New measurements of the flow-curves for Carbopol dispersions without slip artefacts, *Rheol. Acta* 40 (2001) 499.
- [44] L. Baudonnet, J.L. Grossiord, F. Rodriguez, Effect of dispersion stirring speed on the particle size distribution and rheological properties of three carbomers, *J. Dispersion Sci. Tech.* 25 (2004) 183.
- [45] S.J. Curran, R.E. Hayes, A. Afacan, M.C. Williams, P.A. Tanguy, Properties of carbopol solutions as models for yield stress fluids, *J. Food Sci.* 67 (2002) 176.
- [46] P. Sollich, F. Lequeux, P. Hébraud, M.E. Cates, Rheology of soft glassy materials, *Phys. Rev. Lett.* 78 (1997) 2020.
- [47] M. Cloitre, R. Borrega, L. Leibler, Rheological aging and rejuvenation in microgel pastes, *Phys. Rev. Lett.* 85 (2000) 4819.
- [48] Duke Scientific Inc., <http://www.dukescientific.com>.
- [49] J.C. Crocker, D.G. Grier, Methods of digital video microscopy for colloidal studies, *J. Coll. Interf. Sci.* 179 (1996) 298.
- [50] E. Weeks, J.C. Crocker, Particle tracking using IDL, <http://www.physics.emory.edu/~weeks/idl/>.
- [51] D.S. Martin, M.B. Forstner, J.A. Kas, Apparent subdiffusion inherent to single particle tracking, *Biophys. J.* 83 (2002) 2109.
- [52] W.K. Kegel, A. van Blaaderen, Direct observation of dynamical heterogeneities in colloidal hard-sphere suspensions, *Science* 287 (2000) 290.
- [53] B. Doliwa, A. Heuer, Cage effect, local anisotropies, and dynamic heterogeneities at the glass transition: a computer study of hard spheres, *Phys. Rev. Lett.* 80 (1998) 4915.
- [54] E.R. Weeks, D.A. Weitz, Subdiffusion and the cage effect studied near the colloidal glass transition, *Chem. Phys.* 284 (2002) 361; E.R. Weeks, D.A. Weitz, Properties of cage rearrangements observed near the colloidal glass transition, *Phys. Rev. Lett.* 89 (2002) 095704.
- [55] F. Oppong, J.R. de Bruyn, unpublished.
- [56] J.C. Crocker, M.T. Valentine, E.R. Weeks, T. Gisler, P.D. Kaplan, A.G. Yodh, D.A. Weitz, Two-point microrheology of inhomogeneous soft materials, *Phys. Rev. Lett.* 85 (2000) 888.
- [57] A.J. Levine, T.C. Lubensky, One- and two-particle microrheology, *Phys. Rev. Lett.* 85 (2000) 1774.